

# Watching the growth of aluminum hydroxide nanoparticles from aluminum nanoparticles synthesized by pulsed laser ablation in aqueous surfactant solution

Suulki Lee · Jae Ho Shin · Myong Yong Choi

Received: 1 August 2012 / Accepted: 28 January 2013 / Published online: 9 February 2013  
© Springer Science+Business Media Dordrecht 2013

**Abstract** Aluminum nanospheres were prepared by a pulsed Nd-YAG laser ablation method in aqueous surfactant, cetyltrimethylammonium bromide (CTAB), solutions. In the absence of CTAB but with aging, fast hydrolysis reaction between Al and water changed the composition and structures of Al nanospheres to Al oxides and then further to Al hydroxides, bayerite and gibbsite, via a dissolution–recrystallization process. Thus, the control of the hydrolysis rate, producing pure Al and Al hydroxide nanoparticles selectively was attempted by varying the concentration of CTAB in the pulsed laser ablation solution; the transformation processes from Al to Al hydroxides were monitored. The resulting nanoparticles at each development stage were analyzed by X-ray diffraction measurements, field emission scanning electron microscopy, high-resolution transmission electron microscope observations, fast Fourier transform analysis, and energy dispersive spectrometer analysis. Possible mechanisms for the dissolution–recrystallization process of Al hydroxides are proposed.

**Keywords** Al nanoparticles · Al oxide nanoparticles · Al hydroxide nanoparticles · Pulsed laser ablation in liquid (PLAL) · Cetyltrimethylammonium bromide (CTAB)

## Introduction

The exothermic and spontaneous reaction of Al and water has intrigued researchers for many years in the context of hydrogen generation, the commercial blasting industry, and new developments in the renewable energy (Czech and Troczynski 2010; Shimojo et al. 2010; Steinfeld 2005). While thermodynamics of Al reactions predicts that Al reacts with water to generate heat and aluminum hydroxides, in practice a piece of Al dropped into water will not react at room temperature or even with boiling water. This is because the surface of Al is coated with a thin layer of aluminum oxide (alumina,  $\text{Al}_2\text{O}_3$ ), and this is unaffected by water (Weingart 1947); further any reaction is “self-stopping” (Fedoroff 1960) due to the formation of such an impervious film of alumina. Over the many years, alumina has drawn much attention due to its notable physical and chemical properties that include its chemical inertness, and a high melting temperature. As a consequence it has been employed in a wide range of applications spanning catalysts, coatings, and microelectronics (Mezzasalma et al. 2009). However, it is now generally appreciated that the chemical reactivity at the nanometer scale differs from that of macroscopic

---

S. Lee · M. Y. Choi (✉)  
Department of Chemistry and Research Institute  
of Natural Science, Gyeongsang National University,  
Jinju 660-701, Republic of Korea  
e-mail: mychoi@gnu.ac.kr

J. H. Shin (✉)  
Department of Chemistry, Kwangwoon University,  
Seoul 139-701, Republic of Korea  
e-mail: jhshin@kw.ac.kr

counterparts (Henz et al. 2010; Valden et al. 1998; Yang et al. 2004; Yoon et al. 2005). For example, the catalytic and reaction behavior of Al and alumina are known to be size dependent (Reber et al. 2010; Roach et al. 2009). Motivated by this, the structures and morphologies related to the chemical reactivity of Al and alumina at the nanoscale appeared worthy of investigation.

Recently, it has been shown that mixtures of Al and alumina powders are very reactive and, for example, produce hydrogen on reaction with water (Chaklaser 2003; Czech and Troczynski 2010). Furthermore, the hydrolysis of alumina involving Al–O–Al bond breaking has been well established to result in Al–OH species (Bunker et al. 2002; Deng et al. 2007). Further hydrolysis, along with aging, produces hydroxide species in the form of bayerite [Al(OH)<sub>3</sub>] and boehmite [AlO(OH)]; both of these are thermodynamically more stable than alumina at room temperature (Deng et al. 2007). Moreover, the aluminum hydroxide species have different morphologies, such as conical (bayerite), rectangular (gibbsite), and fibrous (boehmite), and their transformations between different hydroxides have been investigated (Lee et al. 1999; Violante and Huang 1993). A number of investigations of the reactivity of the Al–water system have been carried out in the presence of reaction promoters, including NaOH (hydroxide promoter) (Czech and Troczynski 2010), Al<sub>2</sub>O<sub>3</sub> (oxide promoter) (Deng et al. 2007, 2005a, b), and NaCl (salt promoter) (Czech and Troczynski 2010). These promoters act by interrupting the aluminum oxide layer on the Al metal.

In our previous studies, we have reported on the production of Al and  $\gamma$ -Al<sub>2</sub>O<sub>3</sub> nanoparticles via a pulsed Nd-YAG laser in deionized water in the absence of a surfactant or catalyst (Lee et al. 2012a, b). The pulsed laser ablation in liquid (PLAL) (Patil et al. 1987), introduced by Patil and co-workers in 1987, has been demonstrated to be an effective, simple, and versatile method of synthesizing nanomaterials with an appropriate choice of solids and liquids (Liang et al. 2003; Mafuné et al. 2000a; Niu et al. 2010; Yang 2007; Zeng et al. 2005; Zhang et al. 2002). Because of the relatively “simple and clean” preparation of nanoparticles using PLAL, many different metal nanostructures have been fabricated showing desired functional, morphological, and structural properties. The fact that no other chemicals are needed is the major merit of PLAL, especially for

the preparation or transformation of ultrapure nanoparticles.

In this study, hydrolysis of generated Al and  $\gamma$ -Al<sub>2</sub>O<sub>3</sub> nanoparticles coupled with aging to form hydroxides in the absence of surfactants was observed. Thus we were successful in synthesizing specific nanoparticles of Al and Al hydroxides by varying the concentration of surfactant, cetyltrimethylammonium bromide (CTAB) present in the aqueous solution. Furthermore, we monitored a dissolution–recrystallization process of Al nanoparticles produced via PLA in various concentrations of CTAB. Given that a surfactant assisted preparation of specific nanoparticles is found to be an efficient method for the preparation of specific nanoparticles, for example, by the fast hydrolysis of Al and Al oxides, we have investigated the growth process of Al hydroxides with an aid of CTAB.

## Experimental section

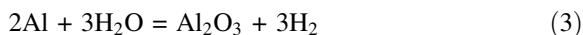
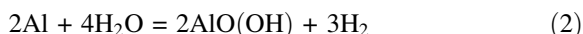
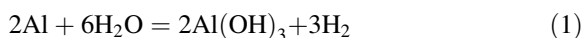
A solid Al (99.999 %, Sigma-Aldrich) plate was ablated by pulsed nanosecond laser in pure water and various concentrations of cetyltrimethylammonium bromide (CTAB, 95 %, Sigma-Aldrich). The concentration of CTAB was adjusted to below, near, and above the critical micelle concentration (CMC). In this work, 0.1, 0.01, 0.005, 0.001, and 0.0001 M CTAB were used to control the hydrolysis rate of the Al nanoparticles.

The experimental set up is described in detail elsewhere (Mafuné et al. 2000a; Sasaki et al. 2006; Zeng et al. 2007). Briefly, the Al plate was fixed in a Pyrex vial filled with deionized water and aqueous CTAB solution (10 mL) continuously stirred by a magnetic bar. A pulsed Nd:YAG laser (1,064 nm, 10 Hz, 7 ns) was focused onto the surface of the Al metal plate with a spot size of about 1 mm in diameter using a lens with a focal length of 25 mm. The laser ablation lasted for 10 min with a laser pulse energy of 50 mJ/pulse. The colloidal solutions were separated at a centrifugation rate of 6,000 rpm for 10 min; the resulting sediment was collected and then sonicated after an addition of the required concentration of CTAB solution, then centrifuged a number of times. The repetition was performed for at least 10 times and the respective sediments were collected and dried on a silicon substrate or a copper grid at room temperature.

The morphology and structure of the nanoparticles produced by PLAL were studied with a field emission scanning electron microscope (FE-SEM, XL30 S FEG, Philips), a transmission electron microscope [TEM, JEOL, JEM-2-10 (200 kV)], a high-resolution transmission electron microscope [HRTEM, TECNAI, TF30ST (300 kV)], and fast Fourier transform (FFT) analysis (GATAN, Inc.). Energy dispersive spectrometer (EDS) analysis was attained using an INCA M/X detector (OXFORD) from 0–20 keV. X-ray diffraction (XRD) patterns of the nanoparticles were obtained with a Bruker AXS D8 DISCOVER with GADDS diffractometer using Cu K $\alpha$  (0.1542 nm) radiation with Bragg angle ranging from 20° to 90°.

## Results and discussion

Near room temperature, the reactions between Al and water to form aluminum oxide and hydroxide are the followings:



In fact, all these reactions are thermodynamically favorable from room temperature to the melting temperature of Al ( $\sim 660$  °C). It is known that (1) is favored from room temperature to 280 °C, while AlO(OH) is the most stable product in the range of 280–480 °C. Above 480 °C, Al<sub>2</sub>O<sub>3</sub> is the most stable product (3) according to the thermodynamics of Al-water reaction (Deng et al. 2005a, b, 2007). In our previous studies (Lee et al. 2012a, b), Al and  $\gamma$ -Al<sub>2</sub>O<sub>3</sub> nanoparticles were produced via the PLAL method by ablating an Al metal plate in deionized water in the absence of any surfactant or catalyst.

The extreme experimental conditions in the plasma plume, such as high temperature ( $\sim 6,000$  K) and pressure ( $\sim 1$  GPa) (Zeng et al. 2005), may have played an important role in the production of Al and  $\gamma$ -Al<sub>2</sub>O<sub>3</sub> nanoparticles in water using the laser ablation method. Especially, it is known that the metastable  $\gamma$ -Al<sub>2</sub>O<sub>3</sub> nanoparticles can be formed when the cooling rate is faster than 100 deg/s (Levi et al. 1988); thus, the much faster cooling rate in PLA provides a likely environment for the production of  $\gamma$ -Al<sub>2</sub>O<sub>3</sub>. The detailed formation mechanisms and characterizations

for the above systems have been discussed previously (Lee et al. 2012a, b). Briefly, Al<sup>3+</sup> ions produced via PLAL onto the Al plate were rapidly cooled by the solution upon the condensation of the laser-induced plasma and eventually forming nanoparticles via agglomeration (Lee et al. 2012a). The preformed Al and  $\gamma$ -Al<sub>2</sub>O<sub>3</sub> nanoparticles will undergo severe hydrolysis, as confirmed by Lee et al. (1999) by observing the aging of bayerite, and gibbsite particles in aqueous solution. Thus, we introduced a surfactant, CTAB, into the PLA solution in an attempt to produce pure Al and Al hydroxide nanoparticles selectively by controlling the hydrolysis rate of Al and Al<sub>2</sub>O<sub>3</sub> nanoparticles, since CTAB has been found to act as a templating-micelle and capping surfactant in the fabrication of mesoporous materials and for controlling some chemical reactions (Besson et al. 2000; Cai et al. 2001; Grosso et al. 2000).

In order to characterize the compositions and structures of the nanoparticles prepared at different CTAB concentrations, a study of XRD patterns of the respective products was conducted. Typical XRD patterns of the nanostructures obtained from Al metal at different CTAB concentrations (0.1, 0.01, 0.005, 0.001, and 0.0001 M) with aging for 3 days are shown in Fig. 1a–e, respectively. At least three different shapes (sphere, triangle, and rectangle) of the product nanostructures were observed under different CTAB concentrations. At the 0.1 M CTAB concentration, about 10<sup>2</sup> times of the critical micelle concentration (CMC) of CTAB (0.98 mM), pure Al nanoparticles, marked by squares, were only present (JCPDS number: 00-004-0787) (Fig. 1a). The XRD pattern of pure Al nanoparticles in 0.1 M CTAB concentration was not changed in the course of aging over at least 1 month. When the CTAB concentration was decreased to 0.01 M, see Fig. 1b, apart from the diffraction peaks for Al, the typical XRD pattern of  $\gamma$ -Al<sub>2</sub>O<sub>3</sub> (JCPDS number: 01-075-0921), marked by circles, was observed. It seemed that the Al atoms on the Al nanosphere surface had started to react with water molecules through the CTAB surfactant layers. When the CTAB concentration was further decreased to 0.005 M, the XRD pattern of pure Al crystals had completely disappeared and a new pattern, marked by triangles, had grown in the diffraction angle range between 15° and 45°, as shown in Fig. 1c. Rather broad backgrounds underneath the bands indicated by triangles in Fig. 1c indicate that the Al(OH)<sub>3</sub> crystals might

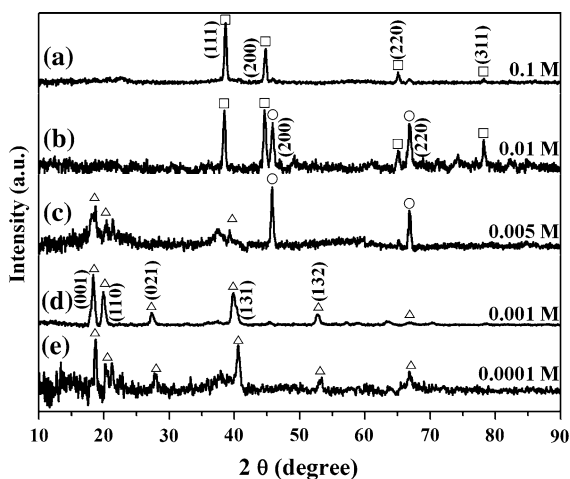
be in the growth process from the amorphous materials, which is also reflected in the following SEM and TEM observations. When the CTAB concentration lies both near and well below the CMC of CTAB [(0.001 M, d) and (0.0001 M, e), respectively], aluminum hydroxide [bayerite,  $\text{Al}(\text{OH})_3$ ] type nanostructures (JCPDS number: 01-074-1119), marked by triangles in Fig. 1d and e, were only present. Based on the XRD results, CTAB is clearly capable of decreasing the hydrolysis rate by reducing the proximity of water to the active Al atoms on the surface of the Al nanoparticles, producing pure Al nanoparticles in the aqueous solutions.

Figures 2 and 3 show typical SEM and TEM images of the nanoparticles generated at the same CTAB concentration as the above experiment. It is interesting to see that the nanoparticles in Figs. 2 and 3a–e are present in their different shapes and sizes. As mentioned before, the spherical Al and  $\gamma\text{-Al}_2\text{O}_3$  nanoparticles changed to a conical shape reflecting the hydrolysis reaction with water after a prolonged time. In order to control the hydrolysis rate of the nanoparticles in water, different concentrations of CTAB were applied to the samples. As shown in Fig. 2a (0.1 M CTAB), all the Al particles are spherical and stayed spherical shapes even after 1 month. The TEM image, shown in Fig. 3a, is also in accord with their spherical shape. When the CTAB concentration was lowered to 0.01 M, several cracked and hollow-type nanoparticles were now apparent

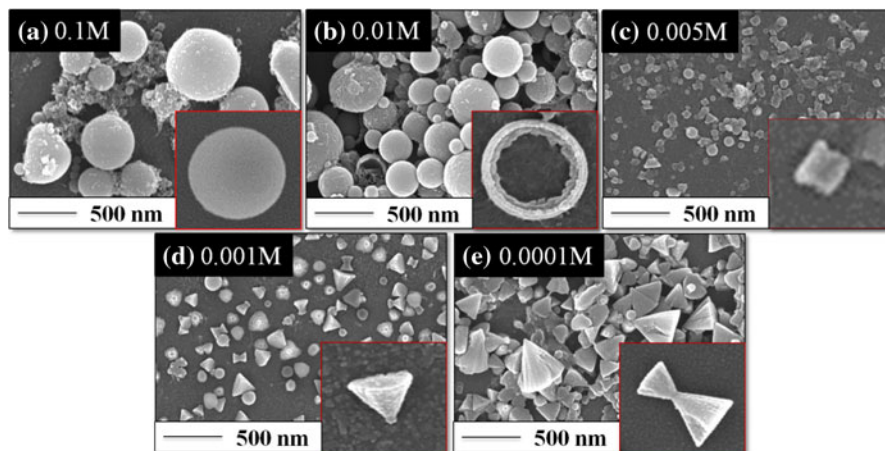
(Fig. 2b); for clarity, an enlarged image is shown in the inset of Fig. 2b. Some hollow spherical nanoparticles are evident in the TEM image given in Fig. 3b. It can thus be concluded that the formation of hollow and cracked particles begins with hydrolysis involving Al-water interactions to form  $\text{Al}_2\text{O}_3$  and this then provides nucleation for further hydrolysis, such that the oxidized surface layers become thicker, which facilitates the erosion process.

From the XRD studies at 0.005 M CTAB concentration, Al nanoparticles were first oxidized to  $\gamma\text{-Al}_2\text{O}_3$  and further hydrolysis proceeded; so that both  $\gamma\text{-Al}_2\text{O}_3$  and  $\text{Al}(\text{OH})_3$  nanocrystals were present together. The SEM and TEM images, shown in Figs. 2c and 3c, respectively, show that the spherical nanoparticles have almost disappeared and size of the observed nanoparticles was greatly reduced; namely, rather shapeless small particles and amorphous materials appeared. This might be due to the severe hydrolysis of the nanoparticles at 0.005 M CTAB concentration. As seen in Figs. 2 and 3c, some particles are in the process of developing and some are in their amorphous state, so that the shapes are not defined; this is supported by the XRD study (Fig. 1c) in which the XRD pattern of  $\text{Al}(\text{OH})_3$  is not very clear compared to that of  $\gamma\text{-Al}_2\text{O}_3$ .

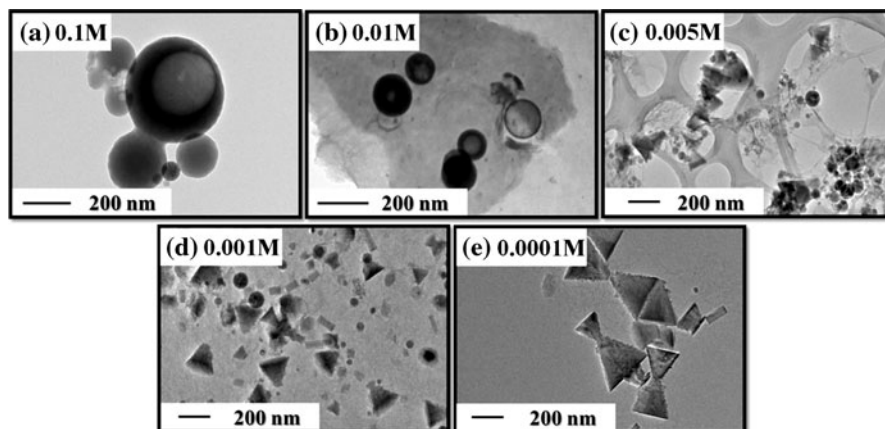
Under the 0.001 M CTAB conditions, the conical nanoparticles are formed fully shaped, Fig. 2d, due to the fact that the hydrolysis reaction has not been significantly deferred by the CTAB concentration employed. At much lower concentration of CMC of CTAB, larger conical nanoparticles are grown either by agglomeration from several nearby conical nanoparticles and/or by self-aggregation, as shown in Fig. 2e. Thus, the size of the conical nanoparticles shown in Fig. 2e has been increased, which is also confirmed by the TEM images given in Fig. 3d and e. Bow-tie shapes are clearly seen in Fig. 3e due to the joining of two conical nanoparticles during growth. Furthermore, some rectangular shaped crystals are also seen in Fig. 3d. Previously, the rectangular crystals were identified to be gibbsite,  $\text{Al}(\text{OH})_3$  (Lee et al. 1999). It is also interesting to note that the sizes of the nanoparticles decrease from (a) to (c) but increase from (c) to (e) (Fig. 2). The results are in keeping with the formation of the Al hydroxides, bayerite (conical shape) and gibbsite (rectangular shape), being accomplished by a dissolution–recrystallization process.



**Fig. 1** XRD patterns of the Al (squares),  $\gamma\text{-Al}_2\text{O}_3$  (circles), and  $\text{Al}(\text{OH})_3$ , bayerite, (triangles) nanoparticles produced by PLA at a power of 50 mJ/pulse in CTAB at concentrations of (a) 0.1, (b) 0.01, (c) 0.005, (d) 0.001, and (e) 0.0001 M



**Fig. 2** FE-SEM images of nanoparticles produced PLAL in CTAB concentration of **a** 0.1, **b** 0.01, **c** 0.005, **d** 0.001, and **e** 0.0001 M. The insets are enlarged views of the typical shape



**Fig. 3** TEM images of nanoparticles produced PLAL in CTAB concentrations of **a** 0.1, **b** 0.01, **c** 0.005, **d** 0.001, and **e** 0.0001 M

The HRTEM images and the corresponding FFT patterns for the Al and Al hydroxide nanoparticles via PLAL at different concentrations of CTAB are presented in Fig. 4. In the HRTEM image of Fig. 4a and b, the measured lattice space is approximately 2.33 and 1.99 Å, consistent with the distance of (111) and (200) planes of pure Al and  $\gamma$ -Al<sub>2</sub>O<sub>3</sub> nanocrystals, respectively. The FFT analysis (insets) of the HRTEM images is identical to the XRD patterns presented in Fig. 1a and b. We were not able to obtain the XRD pattern of gibbsite because of the relatively fewer amounts produced in the samples, as confirmed in Figs. 2 and 3. Nonetheless, we obtained the FFT pattern for the gibbsite crystals from the HRTEM image of Fig. 4c, since the FFT image is able to

provide the information of a very small area compared to the XRD experiment. FFT pattern (upper inset of Fig. 4c) performed on an individual nanorectangle (bottom inset of Fig. 4c) by aligning the electron beam perpendicular to the nanorectangle proves that the nanorectangle is in crystalline phase. The measured lattice spaces of 3.30 and 4.85 Å in the HRTEM image in Fig. 4c are identical to the reference values for (11-2) and (002) planes of gibbsite diffraction angles (JCPDS # 00-033-0018). Figure 4d shows the HRTEM image of the conical nanoparticles, bayerite. The lattice spacing of 4.37 Å for (110) planes of bayerite was resolved on the magnified HRTEM image of the conical wall inset of Fig. 4d. FFT pattern of the nanocorn (bottom inset in Fig. 4d) is also


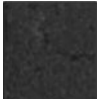
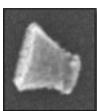



consistent with the phase assignment by XRD (Fig. 1d and e).

In order to characterize the compositions of the various nanoparticles produced at different CTAB concentrations, EDS analysis, as shown in Table 1, was carried out for each of the samples. EDS spectra (not shown) were analyzed to obtain the composition percentages of Al and O atoms in the various shaped nanoparticles. The energies of Al and O atom were 1.44 and 0.46 keV, respectively. The intensity ratios, Al:O, of spherical (a) and amorphous (b) shapes were found to be both about 2:3, which supports the formula  $\text{Al}_2\text{O}_3$ . For the cases of (c) and (d), the intensity ratios of conical (bayerite) and rectangular (gibbsite), respectively, were shown to be both about 1:3, as required for  $\text{Al}(\text{OH})_3$ .

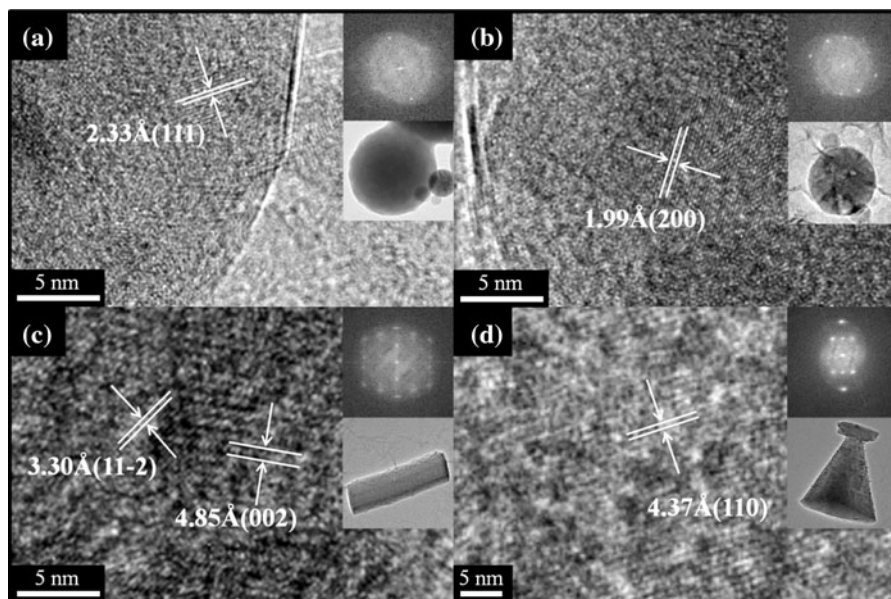
Based on the above results, CTAB has been shown to play an important role as a hydrolysis-deferring agent via coating the surface of Al nanoparticles. In the absence of CTAB, Al atoms on the surface of Al nanoparticles react with water to form Al oxides and further hydrolysis produces Al hydroxides. However, in the presence of surfactant, CTAB acts as a barrier to the approach of water to the surface. We have also demonstrated that the hydrolysis rate is dependent on the concentration of CTAB present. That is, at high

**Table 1** Al and O atom percentages obtained from EDS analysis of Al oxides and hydroxides

Type	Structure		% Al	% O
(a) $\text{Al}_2\text{O}_3$	Spherical		37.04	62.96
(b) Amorphous $\text{Al}_2\text{O}_3$	–		35.76	64.24
(c) Bayerite $\text{Al}(\text{OH})_3$	Conical		23.19	76.81
(d) Gibbsite $\text{Al}(\text{OH})_3$	Rectangular		22.87	77.13

The corresponding SEM image from EDS analysis is shown in each case

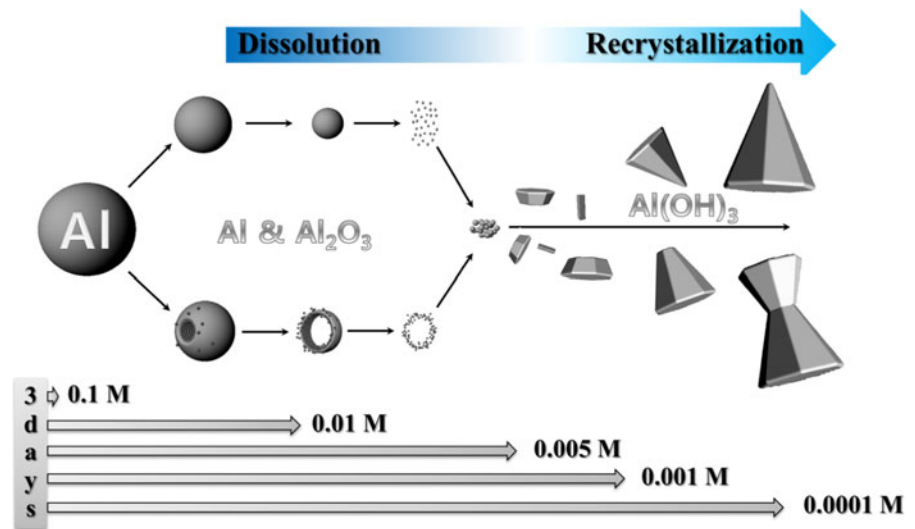
CTAB concentration, water has difficulty in penetrating a bilayer hydrophobic tail of CTAB surrounding the nanoparticle; thereby, intact Al nanoparticles remain unhydrolysed due to the CTAB bilayer and perhaps the surface micelles on the particle surface (Mafuné et al. 2000a, b). However, when the



**Fig. 4** HRTEM images of the nanoparticles of **a** pure Al (JCPDS # 00-004-0787), **b**  $\gamma\text{-Al}_2\text{O}_3$  (JCPDS # 01-075-0921), **c** gibbsite (JCPDS # 00-033-0018), and **d** bayerite (JCPDS #

01-074-1119). (Insets FFT and magnified TEM images of the corresponding nanoparticles)

**Fig. 5** Schematic illustration of the dissolution–recrystallization process of Al nanospheres. Each arrow for the corresponding CTAB concentration is scaled to 3 days



concentration of CTAB becomes lower, the penetration rate of water through the CTAB layers increases; thus water becomes an active role in the hydrolysis of the Al nanoparticles and further induces the erosion process of Al nanospheres. However, in this study, we have observed that the oxide layer induces further hydrolysis with water as an oxide promoter (Deng et al. 2007, 2005a, b) leading to the production of the hydroxide crystals via an erosion process. Therefore, the nanospheres produced at the first stage of PLAL become smaller in the course of the erosion processes; and cracked and/or eroded nanospheres become visible. As the hydrolysis further proceeds further, the nanoparticles are further dissolved to yield shapeless particles along with new types of crystals, namely bayerite and gibbsite, which crystallize in their characteristic shapes (see Fig. 5).

In this study, we have selectively synthesized the Al and Al hydroxide nanoparticles via employing a pulsed Nd-YAG laser and different concentrations of CTAB. Furthermore, we observed growth processes giving rise to the various shapes of Al oxide and hydroxides. At high CTAB concentrations, only pure Al nanoparticles were formed due to the fact that a bilayer of hydrophobic tails of CTAB blocks the water molecules from reacting with the Al nanospheres. As the concentration of CTAB becomes lower, the hydrophobic layers of CTAB become thinner so that water molecules become more likely to penetrate the layer and react with the surface Al atoms, producing Al oxide surface layers. The hydrolysis rates become faster when the concentration of CTAB is much lower

than the CMC of CTAB; thus, a fast erosion process leads to the nanospheres dissolving followed by occurrence of a recrystallization process. The resulting nanoparticles at each stage were analyzed by XRD measurements, SEM, HRTEM, FFT, and EDS analysis. Finally, in the present study PLAL has been confirmed to be simple and clean nanofabrication tool for obtaining specific nanomaterials in the presence of a surfactant. Such a process appears to show promise for the industrial production of metal and metalloid oxide and hydroxide nanomaterials.

**Acknowledgments** This work was supported by the National Research Foundation (KRF) Grant funded by the Korea Government (MEST) (2010-0005493, 2012R1A2A2A02013 289) and Korea Ministry of Environment as “GAIA Project” (2012000550026). J. H. Shin also acknowledges the support from the NRF funded by MEST (2010-0005532) and a Grant from Kwangwoon University.

## References

- Besson S, Ricolleau C, Gacoin T, Jacquiod C, Boilot J-P (2000) A new 3D organization of mesopores in oriented CTAB silica films. *J Phys Chem B* 104:12095–12097
- Bunker BC, Nelson GC, Zavadil KR, Barbour JC, Wall FD, Sullivan JP, Windisch CF, Engelhardt MH, Baer DR (2002) Hydration of passive oxide films on aluminum. *J Phys Chem B* 106:4705–4713
- Cai Q, Luo Z-S, Pang W-Q, Fan Y-W, Chen X-H, Cui F-Z (2001) Dilute solution routes to various controllable morphologies of MCM-41 silica with a basic medium. *Chem Mater* 13:258–263
- Chaklaser A (2003) Hydrogen generation from water split reaction, The University of British Columbia, U.S

- Czech E, Troczynski T (2010) Hydrogen generation through massive corrosion of deformed aluminum in water. *Int J Hydrogen Energy* 35:1029–1037
- Deng Z-Y, Liu Y-F, Tanaka Y, Ye J, Sakka Y (2005a) Modification of Al particle surfaces by  $\gamma$ -Al<sub>2</sub>O<sub>3</sub> and its effect on the corrosion behavior of Al. *J Am Ceram Soc* 88:977–979
- Deng Z-Y, Liu Y-F, Tanaka Y, Zhang H-W, Ye J, Kagawa Y (2005b) Temperature effect on hydrogen generation by the reaction of  $\gamma$ -Al<sub>2</sub>O<sub>3</sub>-modified Al powder with distilled water. *J Am Ceram Soc* 88:2975–2977
- Deng Z-Y, Ferreira JMF, Tanaka Y, Ye J (2007) Physicochemical mechanism for the continuous reaction of  $\gamma$ -Al<sub>2</sub>O<sub>3</sub>-modified aluminum powder with water. *J Am Ceram Soc* 90:1521–1526
- Fedoroff BT (1960) Encyclopedia of explosives and related items. Picatinny Arsenal, New York, p A 143
- Grosso D, Balkenende AR, Albouy PA, Lavergne M, Mazerolles L, Babonneau F (2000) Highly oriented 3D-hexagonal silica thin films produced with cetyltrimethylammonium bromide. *J Mater Chem* 10:2085–2089
- Henz BJ, Hawa T, Zachariah MR (2010) On the role of built-in electric fields on the ignition of oxide coated nanoaluminum: ion mobility versus Fickian diffusion. *J Appl Phys* 107:024901
- Lee Y-P, Liu Y-H, Yeh C-S (1999) Formation of bayerite, gibbsite and boehmite particles by laser ablation. *Phys Chem Chem Phys* 1:4681–4686
- Lee S, Ahn A, Choi MY (2012a) Direct observation of aluminum ions produced via pulsed laser ablation in liquid: a 'turn-on' fluorescence study. *Phys Chem Chem Phys* 14:15677–15681
- Lee S, Jung HJ, Shin JH, Choi MY (2012b) Size distribution of aluminum and alumina nanoparticles produced via pulsed laser ablation of aluminum plate in water: laser power dependence. *J Nanosci Nanotechnol* 12:8900–8903
- Levi CG, Jayaram V, Valencia JJ, Mehrabian R (1988) Phase selection in electrohydrodynamic atomization of alumina. *J Mater Res* 3:969–983
- Liang C, Shimizu Y, Sasaki T, Koshizaki N (2003) Synthesis of ultrafine SnO<sub>2-x</sub> nanocrystals by pulsed laser-induced reactive quenching in liquid medium. *J Phys Chem B* 107:9220–9225
- Mafuné F, Kohno J-y, Takeda Y, Kondow T, Sawabe H (2000a) Formation and size control of silver nanoparticles by laser ablation in aqueous solution. *J Phys Chem B* 104:9111–9117
- Mafuné F, Kohno J-y, Takeda Y, Kondow T, Sawabe H (2000b) Structure and stability of silver nanoparticles in aqueous solution produced by laser ablation. *J Phys Chem B* 104:8333–8337
- Mezzasalma AM, Mondio G, Serafino T, Caridi F, Torrisi L (2009) Electronic properties of thin films of laser-ablated Al<sub>2</sub>O<sub>3</sub>. *Appl Surf Sci* 255:4123–4128
- Niu KY, Yang J, Kulinich SA, Sun J, Li H, Du XW (2010) Morphology control of nanostructures via surface reaction of metal nanodroplets. *J Am Chem Soc* 132:9814–9819
- Patil PP, Phase DM, Kulkarni SA, Ghaisas SV, Kulkarni SK, Kanetkar SM, Ogale SB, Bhide VG (1987) Pulsed-laser induced reactive quenching at liquid-solid interface: aqueous oxidation of iron. *Phys Rev Lett* 58:238–241
- Reber AC, Khanna SN, Roach PJ, Woodward WH, Castleman AW (2010) Reactivity of aluminum cluster anions with water: origins of reactivity and mechanisms for H<sub>2</sub> release. *J Phys Chem A* 114:6071–6081
- Roach PJ, Woodward WH, Castleman AW, Reber AC, Khanna SN (2009) Complementary active sites cause size-selective reactivity of aluminum cluster anions with water. *Science* 323:492–495
- Sasaki T, Shimizu Y, Koshizaki N (2006) Preparation of metal oxide-based nanomaterials using nanosecond pulsed laser ablation in liquids. *J Photochem Photobiol A* 182:335–341
- Shimojo F, Ohmura S, Kalia RK, Nakano A, Vashishta P (2010) Molecular dynamics simulations of rapid hydrogen production from water using aluminum clusters as catalyzers. *Phys Rev Lett* 104:126102
- Steinfeld A (2005) Solar thermochemical production of hydrogen—a review. *Sol Energy* 78:603–615
- Valden M, Lai X, Goodman DW (1998) Onset of catalytic activity of gold clusters on titania with the appearance of nonmetallic properties. *Science* 281:1647–1650
- Violante A, Huang PM (1993) Formation mechanism of aluminum hydroxide polymorphs. *Clays Clay Miner* 41:590–597
- Weingart G (1947) Pyrotechnics, 2nd edn. Chemical Publishing Company, New York
- Yang GW (2007) Laser ablation in liquids: applications in the synthesis of nanocrystals. *Prog Mater Sci* 52:648–698
- Yang Y, Wang S, Sun Z, Dlott DD (2004) Near-infrared laser ablation of poly tetrafluoroethylene (Teflon) sensitized by nanoenergetic materials. *Appl Phys Lett* 85:1493–1495
- Yoon B, Häkkinen H, Landman U, Wörz AS, Antonietti JM, Abbet S, Judai K, Heiz U (2005) Charging effects on bonding and catalyzed oxidation of CO on Au<sub>8</sub> clusters on MgO. *Science* 307:403–407
- Zeng H, Cai W, Li Y, Hu J, Liu P (2005) Composition/structural evolution and optical properties of ZnO/Zn nanoparticles by laser ablation in liquid media. *J Phys Chem B* 109:18260–18266
- Zeng H, Li Z, Cai W, Cao B, Liu P, Yang S (2007) Microstructure control of Zn/ZnO core/shell nanoparticles and their temperature-dependent blue emissions. *J Phys Chem B* 111:14311–14317
- Zhang W, Zhang Y, Tang J, Zhang Y, Wang L, Ling Q (2002) Study on preparation and optic properties of nano europium oxide-ethanol sol by pulsed laser ablation. *Thin Solid Films* 417:43–46